

SEA SURFACE CURRENT FIELDS IN THE BALTIC SEA DERIVED FROM MULTI-SENSOR SATELLITE DATA

Benjamin Seppke^{a,*}, Martin Gade^b and Leonie Dreschler-Fischer^a

^aDepartment Informatik, Universität Hamburg, Hamburg, Germany - (seppke, dreschler)@informatik.uni-hamburg.de

^bInstitut für Meereskunde, Universität Hamburg, Hamburg, Germany - martin.gade@zmaw.de

KEY WORDS: satellite oceanography, remote sensing, multi-sensor, algae blooms, surface currents, optical flow

ABSTRACT:

Mesoscale dynamic sea surface features, such as eddies, fronts, or dipoles, are of key importance for our understanding of local dynamics of the marine coastal environment. However, they are often not fully resolved by numerical models currently in use. Series of satellite images (with resolutions ranging from a few meters to hundreds of meters), acquired within a short time period (from less than an hour to a day), can be used to close this gap, if the spatial and temporal extent of those dynamic surface features fits to the spatial and temporal resolution of the sensors and of the data acquisitions, respectively. Moreover, current tracers that are detectable by all applied sensors, need to be present during the whole time of image acquisitions. In this paper we demonstrate the use of multi-sensor / multi-channel satellite images for the computation of mesoscale surface currents in the Central Baltic Sea. The images were acquired by the Thematic Mapper (TM), the ERS-2 Synthetic Aperture Radar (SAR), the Envisat Advanced SAR, the Wide-Field Scanner (WiFS), and the Sea-viewing Wide Field-of-view Sensor (SeaWiFS) during extensive summer algae (cyanobacterial) blooms in July 1997 (Northern Baltic Proper) and in July / August 1999 (Southern Baltic Proper), and after an oil spillage in May 2005 (north of the Bay of Gdansk). Both natural and man-made surface films affect the sea surface and thus are visible on satellite imagery. We show that, in some cases, data from sensors working at different electromagnetic frequency bands (e.g., TM and SAR) can be used to apply high-speed feature-matching (cross-correlation) techniques for motion detection. In other cases, best results were obtained through the calculation of the optical flow between subsequent images acquired by the same sensor (e.g., WiFS, SeaWiFS, or ASAR). Our computed two-dimensional surface current fields show good agreement with, and they also complement, results from numerical model runs. However, limitations of the proposed methods are due to the strong dependence of the visibility of marine surface films on local weather conditions and to the low availability of satellite data.

KURZFASSUNG:

Mesoskalige Eigenschaften der Meeresoberfläche, wie z.B. lokale Wirbel, Fronten oder Dipole sind für das Verständnis der lokalen Dynamik des Meeres in Küstennähe sehr wichtig. Leider erfassen aktuelle numerische Modelle, die auf größeren Skalen arbeiten, diese Eigenschaften meist nicht oder nur unzeichnend. Allerdings kann mit Serien von Satellitenbildern (wobei die Auflösung von einigen Metern bis hin zu einigen hundert Metern reicht), die innerhalb eines kurzen Zeitraums (von weniger als einer Stunde bis zu einem Tag) aufgenommen wurden, diese Lücke geschlossen werden. Dazu müssen verfolgbare Objekte von den Sensoren erfasst worden sein, die sich nur mit der lokalen Meeresströmung bewegen. In diesem Artikel wird der Einsatz Multi-Sensor und Multi-Spektral-Bildern für die Berechnung der mesoskaligen Oberflächenströmung in der zentralen Ostsee aufgezeigt. Die Bilddaten stammen von dem Landsat Thematic Mapper (TM), dem ERS-2 Synthetic Aperture Radar (SAR), dem Wide-Field Scanner (WiFS) und dem Sea-viewing Wide Field-of-view Sensor (SeaWiFS). Sie wurden während einer ausgedehnten Algenblüte (cyanobacterial) im Juli 1998 im nördlichen Teil der Ostsee, sowie im Juli / August 1999 im südlichen Teil der Ostsee aufgenommen. Ein weiteres Bildpaar zeigt zwei Ölflecken. Es wurde im Mai 2005 von dem Envisat Advanced SAR aufgenommen und stammt aus dem südlichen Teil der Ostsee (nördlich der Danziger Bucht). Sowohl natürliche als auch künstliche Oberflächenfilme beeinflussen die Meeresoberfläche und lassen sich deshalb auch auf der Satellitenaufnahmen wiederfinden. Es wird gezeigt, dass in es in einigen Fällen möglich ist, die Daten verschiedener Sensoren, die auf unterschiedlichen Frequenzen des EM-Spektrums arbeiten, zu kombinieren, um ein sehr schnelles Merkmals-Matching mittels einer optimierten Kreuz-Korrelation durchzuführen. Falls die Satellitendaten von gleichen oder ähnlichen Sensoren stammen, können bessere Ergebnisse durch die Berechnung des Optischen Flusses erreicht werden (z.B. WiFS, SeaWiFS, or ASAR). Die berechneten zweidimensionalen Oberflächen-Strömungsfelder zeigen eine gute Übereinstimmung mit denen numerischer Modelle, verfeinern diese jedoch zudem. Dennoch gibt es leider gewisse Beschränkungen in den vorgeschlagenen Methode, die vor allem im Vorhandensein von Oberflächenfilmen, den lokalen Wetterbedingungen und der geringen Verfügbarkeit von Satellitenbildern begründet sind.

1 INTRODUCTION

Remote sensing data from satellite-borne sensors working at the same or different electromagnetic frequencies can be used to derive ocean current fields, if the same small-scale features are visible in the different data sets and if the data were acquired quasi-simultaneously (i.e., within a certain time period, which depends on the lifetime of the observed features). These features may be driven by the local (surface) currents and the correlation of the

two-dimensional data sets may therefore allow for the calculation of mesoscale ocean current fields. Marine surface films are well suited for such kind of data analyses, because they can change both the sea surface roughness (Gade et al., 1998a) and its emissivity of electromagnetic waves (Kahru et al., 1993). The Baltic Sea is an almost fully enclosed non-tidal brackish water body of about 380,000 km². The summer (July - August) algae blooms in the open Baltic Sea (Figure 1) are often dominated by the species *Nodularia spumigena* and *Aphanizomenon*

sp. These blooms are usually associated with a massive appearance of marine surface films consisting of oily substances that are released by the algae. During the later phase of the bloom, the algae start to flocculate and accumulate on the sea surface in large quantities, thereby becoming visible even with non-optimized satellite sensors (see Figure 2). The surface accumulations of cyanobacteria can cause a higher reflectance of near infrared (NIR) radiation, and in some cases, can cause a local increase in the satellite-derived sea surface temperature (SST) due to increased absorption of sunlight by the higher phytoplankton pigment concentration (Kahru et al., 1993). Thus, multi-sensor satellite data are suitable for the detecting and the tracking of algae blooms. Moreover, if a sufficient amount of satellite data is available, sea surface currents may be derived.

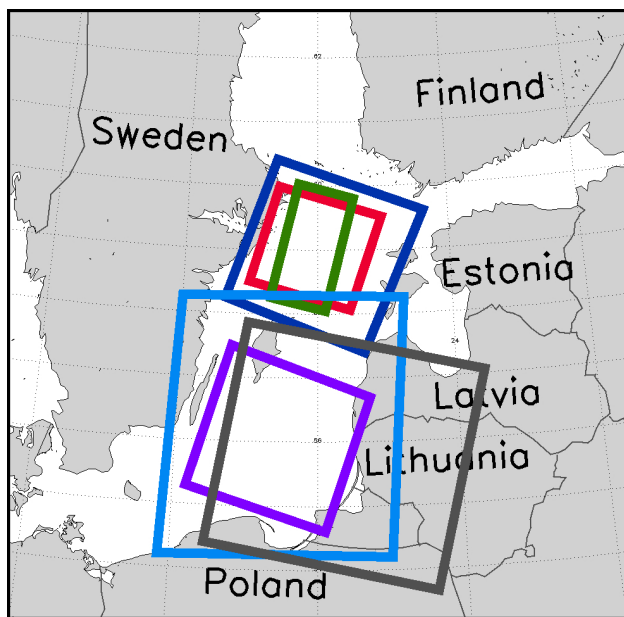


Figure 1: Map of the Central Baltic Sea (Baltic Proper) indicating the location of the used satellite images. July 15, 1997 (Northern Baltic Proper): SAR (green), Landsat TM (red) WiFS (dark blue). July / August, 1999 (Southern Baltic Proper): WiFS (purple) and SeaWiFS (light blue). May 15, 2005 (Southern Baltic Proper): SAR (gray)

2 SATELLITE DATA

In order to demonstrate the applicability of a multi-sensor correlation analysis we used three sets of (non-calibrated) remote sensing data acquired in July 1997 over the Northern Baltic Proper and in July/August 1999 over the Southern Baltic Proper. The images were acquired by various satellite-borne sensors working in the optical, infrared and microwave bands. Figure 1 shows a map of the central Baltic Sea (Baltic Proper) with the geographical locations of the used satellite data inserted.

For the first study presented herein, we have chosen two areas of interest. The first area is the Northern Baltic Proper, north of the Swedish island of Gotland. On July 15, 1997, a day with extensive cyanobacterial blooms in the northern Baltic Proper, data from four different satellite sensors were acquired over the same sea surface area, including the Thematic Mapper (TM, see Figure 2) aboard Landsat, the Synthetic Aperture Radar (SAR) aboard ERS-2 and the Wide-Field Scanner (WiFS) aboard IRS-1C. In Figure 2 a composite of Landsat TM bands 1, 2, and 4, respectively, is shown. The accumulated algae are visible as green structures in most parts of the image.

Another extensive cyanobacterial bloom was encountered in the Southern Baltic Proper, south of Gotland, in late July / early August 1999. During several days of mostly cloud-free weather conditions, more than 70 satellite images of that area were acquired by various optical and microwave sensors, including those from WiFS (acquired on July 30) and from SeaWiFS (acquired on August 1 and 2).

The third pair of images was acquired by the ASAR sensor (in Wide Swath mode) aboard ENVISAT in May 2005. We detected two dark patches off the Bay of Gdansk in these images that are likely to result from oil spills.

The different sensors, the satellite platforms, spatial resolutions (pixel sizes), and acquisition times are given in Table 1. A more detailed description of the available data set can be found elsewhere (Gade et al., 1998b, Rud and Gade, 1999, 2000).

Sensor	Platform	Pixel Size	Acquisition Time
Northern Baltic Proper			
<i>July 15, 1997</i>			
TM	Landsat	30 m	0857 UTC
SAR	ERS-2	12.5 m	0947 UTC
WiFS	IRS-1C	188 m	1026 UTC
Southern Baltic Proper			
<i>July 30, 1999</i>			
WiFS	IRS-1C	188 m	1003 UTC
	IRS-1D		1039 UTC
<i>August 1 & 2, 1999</i>			
SeaWiFS	Sea Star	1.1 km	1003 UTC
			1147 UTC
<i>May 15, 2005</i>			
SAR	Envisat	150 m	0900 UTC
			2025 UTC

Table 1: Satellite sensor characteristics

3 METHODS

The basic idea of the analyses presented herein is to derive motions of the observed brightness patterns (the so-called optical flow) and thus a sea surface current field. Most of the analyzed data show surface accumulations of algae and/or surfactants during ongoing algae blooms. Because of the small penetration depth into water of electromagnetic waves in the (far) red and NIR range, only features in the upper water layer can be detected in these channels. Thus, these bands were used for the computation of mean currents of the upper water layer.

Depending on the imaging characteristics of the build-in sensors and of the amount of available data we have applied different methods: a fast normalized cross-correlation analysis was performed with single-channel data from different sensors (working at different electromagnetic frequencies). A differential method based on the so called Optical Flow Constraint Equation (Horn and Schunck, 1981) was used for (series of) multi-channel data acquired at the same electromagnetic bands and within a short period of time. In this paper, we present examples for each of the methods.

To derive motions even if there is a great spatiotemporal distance between the features, we embedded a technique to estimate the global motion of a scene before starting with the cross-correlation or differential analysis. In order to stabilize the internal gradient calculation of the differential method, we replaced the gradient and average computation proposed by Horn and Schunck (1981) by a Gaussian one that will be described herein after.

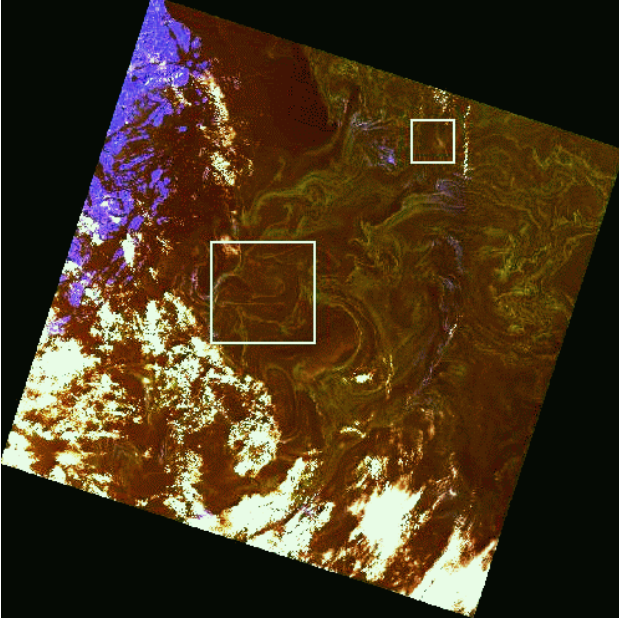


Figure 2: Composite of TM bands 1,2, and 4 showing manifestations of an ongoing algae bloom. Bright patches in the lower half are clouds, blue patches on the left are islands. The squares denote the locations of the used subsets.

3.1 Global Motion Estimation

Before starting the cross-correlation or differential image analysis, we derived the "global motion" for the scene. The underlying idea is that the overall motion can be divided into two parts: A global part which describes the main direction and rotation of movement, and a non-global part, which represents the deviation from the global movement. Obviously, both motion parts sum up to the complete motion. For the estimation of the global displacement we used an efficient implementation of the approach described by Sun (1996). This method allows to reduce the size of the search-window for the normalized cross-correlation because the major part of the motion has already been removed. Likewise, the differential method benefits from this estimation. However, if there is a major structural change of the scene elements, (e.g. fast deforming algae films) this method may fail.

3.2 Maximum Cross-Correlation Analysis

To increase the performance of the normalized cross-correlation, we use the "Fast Normalized Cross-Correlation" method proposed by Lewis (1995). It reduces the computation time of the normalized cross-correlation by using the Fast Fourier Transform to compute the cross-correlation and running sum-tables for the normalization of each cross-correlation result. This type of image analysis is applied for pairs of images acquired by different sensors (i.e., one image or frequency band per sensor) or for pairs of images acquired by the same sensor, if the spatio-temporal distance between the features is too high.

3.3 Differential Method

The differential method is based on the Optical Flow Constraint Equation (Horn and Schunck, 1981), which assumes that the image intensity of the scene elements does not change over time:

$$\frac{dI}{dt} = \frac{\partial I}{\partial x} v_x + \frac{\partial I}{\partial y} v_y + \frac{\partial I}{\partial t} = 0 \Leftrightarrow \nabla I \cdot \vec{v} = -\frac{\partial I}{\partial t} \quad (1)$$

Obviously, the two components of the motion (v_x and v_y) cannot be uniquely derived from this single equation. Horn's and Schunck's approach to solve the optical flow constraint equation is to add an additional constraint. They assume a smoothness of the motion that is controllable by a weighting factor α which leads to a minimization of the motion gradient. Horn and Schunck propose to minimize the functional:

$$E = \int (\nabla I \cdot \vec{v} + I_t)^2 + \alpha^2 \cdot |\nabla \vec{v}|^2 dx dy \quad (2)$$

Minimizing this (convex) functional results in solving the correspondent Euler-Lagrange equations that can be found in (Horn and Schunck, 1981). Horn and Schunck suggest to use Gauss-Seidel iterations for this task which leads to:

$$\vec{v}_{n+1} = \langle \vec{v} \rangle_n - \nabla I \cdot \frac{\nabla I \cdot \langle \vec{v} \rangle_n + I_t}{\alpha^2 + I_x^2 + I_y^2} \quad (3)$$

where I_x , I_y and I_t are the partial derivatives in space and time and $\langle \vec{v} \rangle_n$ denotes the local motion average of the previous step n . The iterative process of minimization leads to the effect of filling-in. In parts of the image where the image gradient is zero, the motion estimates will be filled-in from the neighboring motion estimates. This is necessary, because in there is no local information in these areas that can be used to fulfill the constraint of a smooth motion.

Because we estimate that the real current motion is both smooth and global, we use an adapted version of the algorithm described by Horn and Schunck. To avoid numerical instabilities, we substituted the calculation of the spatial gradients by the convolution with a derived Gaussian filter kernel with standard deviation σ . This allows us to suppress artifacts that were caused by high spatial gradients that were induced by noise. Consequently, we also replaced the proposed local average method by the convolution of Gaussian filter kernel with the same standard deviation σ .

4 RESULTS AND DISCUSSION

First case: July 15, 1997

The first example for deriving surface currents using the cross-correlation method is shown in Figure 3 where data from the SAR and TM sensors have been used. We have chosen microwave (SAR) and NIR (TM band 4), because at both frequency bands the very water surface (or its roughness) is imaged. Although both sensors image the ocean surface films, we cannot use advanced differential approaches in this case, because there is no grey value equivalence between equally imaged objects. Both images were geo-coded and resampled to a pixel size of 30 m, and the SAR image was inverted.

As a first step we have applied a monotonicity operator (Enkelmann et al., 1988) to the TM image, which detects areas of strong algae accumulations as local maxima of the image brightness (monotony classes 7 and 8). Before starting with the correlation analysis, we estimate and correct the global motion between the two images before we calculate the two-dimensional cross-correlation of the surrounding 60 pixel \times 60 pixel area of each detected feature point and the corresponding part of the inverted SAR image (100 pixel \times 100 pixel area). The local maximum of this correlation denotes the most likely (relative) location of the respective feature in the second (SAR) image and was used to determine the final motion vectors.

A typical example of the results of this analysis is shown in Figure 3. The white patches in the background origin from the TM scene, whereas the dark grey patches origin from the (inverted) SAR scene. The arrows are mostly parallel and denote a mean surface speed of about 17 cm/s.

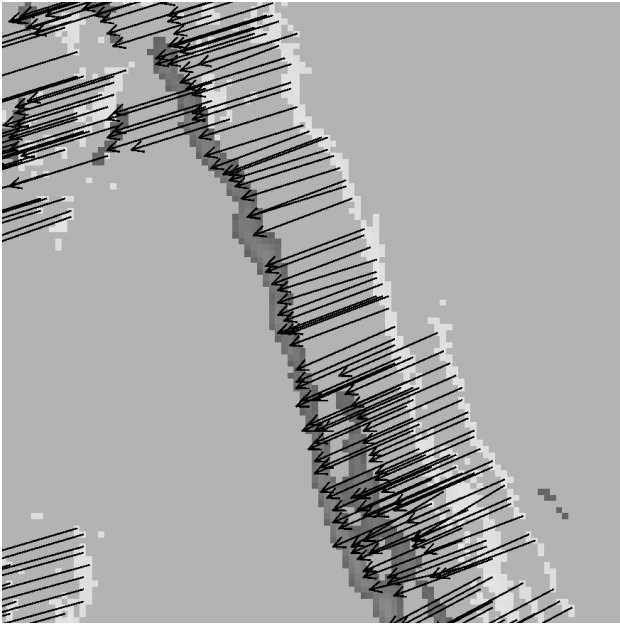


Figure 3: Result of the maximum cross-correlation analysis applied to the TM4 and the SAR scene (see the small square in Figure 2). Features visible in the TM4 scene (white) are spatially shifted in the (inverted) SAR scene (dark grey) by the local current. Image dimensions are $3 \text{ km} \times 3 \text{ km}$.

Second case: July 15, 1997 A first example for surface currents derived using the differential method is shown in Figure 4. The images were acquired on July 15, 1998, by the TM and WiFS sensors, and we chose a sub-scene close to that used for the maximum cross-correlation analysis (see the larger square in Figure 2). Given the imaging properties (i.e., the reflectance) of the detected features were not changing within the period of image acquisition (89 minutes, see Table 1), pairs of images acquired by the two sensors at corresponding electromagnetic bands can be used for the differential method. The images were geo-coded and re-sampled at the lower resolution (188 m pixelsize). The images were acquired at corresponding spectral bands: TM band 3 (0.63-0.69 m) and WiFS band 1 (62-0.68 m). For the calculation of the current field, we used our extended Horn and Schunck algorithm with a standard deviation of the Gaussian filters $\sigma = 1.0$, the smoothing factor $\alpha = 2.0$ and with 200 iterations. The resulting vector field is shown in Figure 4. The most pronounced result is the appearance of high-speed current patterns in the northeast and southeast areas of Figure 4. These patterns result from clouds that exist in the first image but disappeared in the second image.

Third case: July, 1999

In July and August 1999, most parts of the sea surface in the Southern Baltic Proper were covered by algae accumulations (Rud and Gade, 2000). The comprehensive data set acquired over that area between July 27 and August 2 comprises WiFS and SeaWiFS satellite imagery that is suitable for applying the differential method. From this data set we have chosen two pairs of multi-channel satellite images for our analyses. For the differential method, we used band 1 of both acquisitions. The light grey irregular patches in most parts of the image are caused by surface accumulations of cyanobacteria. Because of the short time lag between the two acquisitions (36 minutes) and the spatial resolution of the WiFS sensors (188 m), the minimum surface velocity that can be resolved with this data set is about 2-3 cm/s, which is a realistic value for minimum currents.

For the calculation of the current field, we used the extended

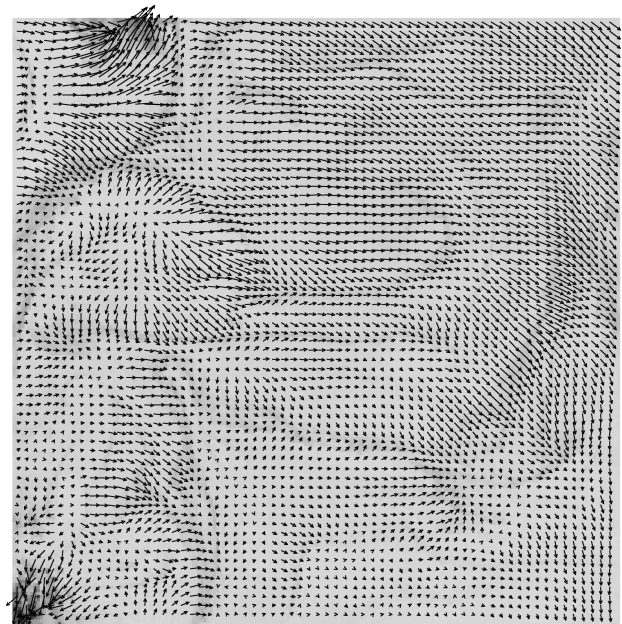


Figure 4: Result of the application of the differential method using pairs of TM and WiFS scenes (see lower square in Figure 2). Image dimensions are $37.6 \text{ km} \times 37.6 \text{ km}$.

Horn and Schunck algorithm with a Gaussian standard deviation $\sigma = 1.0$, a smoothing factor $\alpha = 5.0$, and with 200 iterations. We chose a higher smoothing factor for this pair in order to suppress artificial roughness in the calculated currents that result from grey value changes in the images that do not reflect motions. The result of the differential analysis is shown in Figure 5. The white background corresponds to dark areas in the respective WiFS images, i.e., to areas with low algae accumulation. For the dark areas (where the algae caused pronounced signatures) we calculated realistic surface currents of about 25-35 cm/s.

Fourth case: August, 1999

We used a pair of SeaWiFS images acquired on August 1 and 2, 1999, to investigate if low-resolution satellite imagery is suitable for calculating sea surface currents. We have chosen a $100 \text{ km} \times 200 \text{ km}$ area for which sea surface currents were calculated. For the calculation of the currents, we applied the adapted Horn and Schunck algorithm to band 5 of both acquisitions with a Gaussian standard deviation $\sigma = 1.0$, a smoothing factor $\alpha = 20.0$, and with 200 iterations. Because of the longer time lag between the two image acquisitions (one day), we needed to increase the value of the smoothness factor α . The results of our analysis of the SeaWiFS data are not quite different from those presented before. The daily mean currents calculated using this data set are of the order of 4-10 cm/s.

Fifth case: May 15, 2005

We have also used a pair of ENVISAT SAR Wide Swath-Mode images acquired on May 15, 2005 to find out if low-resolution synthetic aperture radar satellite imagery is suitable for calculating sea surface currents. Both SAR images (09:00 and 20:25 UTC) are showing two oil spills north off the Bay of Gdansk. Because of the great spatiotemporal distance between the features of these images and the structural change of the oil spills, we could not use the optical flow method in this case.

For the detection of the features for which the cross-correlation was calculated, we applied a monotonicity operator to the Gaussian gradient magnitude (at scale $\sigma = 3.0$) of the first image, which detects the border areas of the oil spills as local maxima of

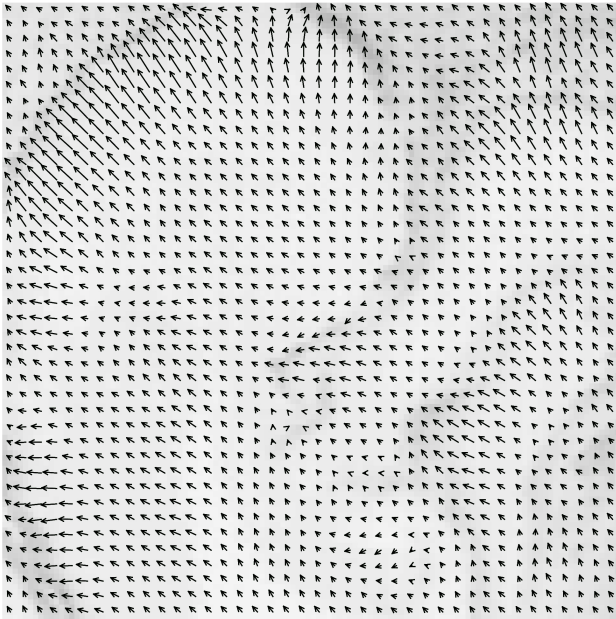


Figure 5: Result of the application of the differential method using a pair of WiFS images. Image dimensions are $22.5 \text{ km} \times 22.5 \text{ km}$.

the image gradient (monotony classes 7 and 8).

After the feature detection, we calculated the two-dimensional cross-correlation of the surrounding $50 \text{ pixel} \times 50 \text{ pixel}$ area of each detected feature point and the corresponding part of the SAR image ($230 \text{ pixel} \times 230 \text{ pixel}$ area). The local maximum of this correlation was used to determine the final motion vectors. A typical example of the results of this analysis is shown in Figure 6. The white patches in the background origin from the oil spills at 0900 UTC, whereas the dark grey patches origin from the oil spills at 2025 UTC. The arrows are mostly parallel and denote a mean surface speed of about 17-28cm/s in accordance with the model results provided by local hydrographic agencies (Kleine, 1994, Funkquist and Kleine, n.d.).

5 CONCLUSIONS

Remote sensing data from satellite-borne sensors working at the same or different electromagnetic frequencies can be used to derive pixel motions that manifest in image brightness variations in the used satellite data.

However, there are some certain aspects that hinder the straightforward use of well-known motion analysis techniques and algorithms in the area of remote sensing. One problem is that the normalized cross-correlation becomes very slow if there is a big spatiotemporal distance between the features of both images. This is caused by a quadratically increasing search space of the mask around each feature. This problem also influences the differential methods, which assume a quite small spatiotemporal distance between two images. Another problem that has to be taken into account for differential methods is that the internal gradient calculation of these methods may become numerically unstable if there is spatial noise and a sparse time axis. Unfortunately, we often encounter these problems in the field of satellite imagery. Almost every image is noisy and the time axis is often sampled with just two images. Therefore, we used the global motion estimation as a preprocessing step and added more numerical stability to the differential methods.

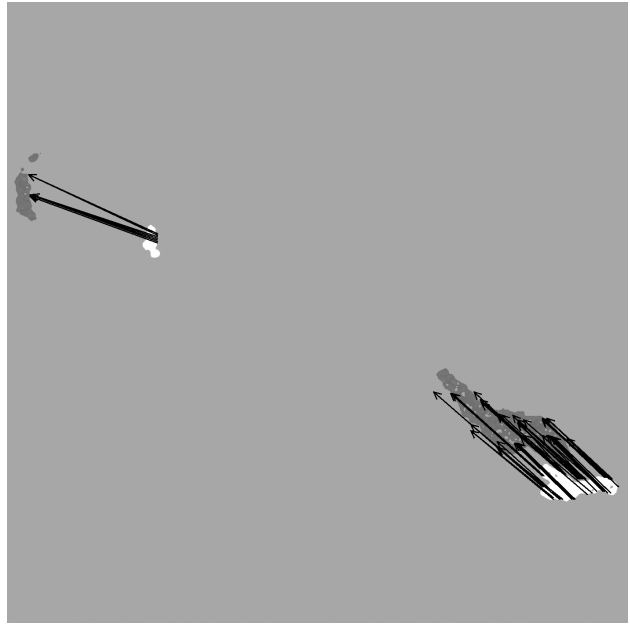


Figure 6: Result of the cross-correlation analysis applied to the SAR scene of the oil spill located north of Gdansk: The oil spills of the first image at 0900 UTC (white) are spatially shifted in the second image at 2025 UTC (dark grey) by the local current. Image dimensions are $60 \text{ km} \times 60 \text{ km}$.

Our first results show that the direct conversion of pixel motions into sea surface currents may be dangerous if data from different sensors were used (e.g., TM and WiFS) or if the spatial resolution with respect to the short time lag between the image acquisitions is too low (WiFS). In these cases, we needed to increase the smoothness parameter of the differential method to avoid irregular current patterns. Another problem is the sensitivity to changes of the image intensity. It seems that not all image intensity changes result from motion, which is the basic assumption of the differential methods presented herein.

Model data are usually not suitable for a direct comparison with our results, if they represent temporal and spatial means of the local currents. However, the comprehensive data set available for the time period of late July / early August, 1999, can be used to produce a series of current maps for large parts of the Southern Baltic Proper, which in turn can be compared with available model data. However, we are aware that any vertical mixing may hinder a successful calculation of sea surface currents by means of signatures of algae accumulations. Also, cloud-free weather conditions are generally necessary for this kind of digital image analysis. The effect of the appearance and disappearance of clouds can be seen in Figure 4. Another approach we presented is to calculate currents from a pair of SAR images, because they do not image clouds. In some cases, two single-channel images acquired, e.g., by SAR and NIR sensors may be sufficient to derive small-scale current fields. However, because of the different imaging of oceanic features by SAR and NIR sensors, this method may fail and the computed currents may be erroneous. Nevertheless, the results shown in Figure 3 are likely to represent the real currents, since both NIR sensor and SAR were detecting algae at the very water surface and the associated damping of surface roughness, respectively (Rud and Gade, 1999).

ACKNOWLEDGEMENTS

The authors are grateful to Ove Rud for his help in allocating the data sets of coinciding satellite images and for placing some of the data at our disposal.

REFERENCES

- Enkelmann, W., Kories, R., Nagel, H. and Zimmermann, G., 1988. An Experimental Investigation of Estimation Approaches for Optical Flow Fields. In: MU88, pp. 189–226.
- Funkquist, L. and Kleine, E., n.d. In manuscript. An introduction to HIROMB, an operational baroclinic model for the Baltic Sea. Technical report, SMHI. Norrköping.
- Gade, M., Alpers, M., Hühnerfuss, H., Masuko, H. and Kobayashi, T., 1998a. The Imaging of Biogenic and Anthropogenic Surface Films by the Multi-frequency Multi-polarization SIR-C/X-SAR. *J. Geophys. Res* (103), pp. 18851–18866.
- Gade, M., Rud, O. and Ishii, M., 1998b. Monitoring algae blooms in the Baltic Sea by using spaceborne optical and microwave sensors. *Geoscience and Remote Sensing Symposium Proceedings, 1998. IGARSS '98. 1998 IEEE International 2*, pp. 754–756.
- Horn, B. K. P. and Schunck, B. G., 1981. Determining Optical Flow. *Artificial Intelligence*.
- Kahru, M., Leppänen, J.-M. and Rud, O., 1993. Cyanobacterial blooms cause heating of the sea surface. *Mar. Ecol. Progr. Ser.* (101), pp. 1–7.
- Kleine, E., 1994. Das operationelle Model des BSH für Nordsee und Ostsee, Konzeption und Übersicht. Technical report, Bundesamt für Seeschifffahrt und Hydrographie. Hamburg.
- Lewis, J. P., 1995. Fast Normalized Cross-Correlation. In: *Vision Interface, Canadian Image Processing and Pattern Recognition Society*, pp. 120–123.
- Rud, O. and Gade, M., 1999. Monitoring algae blooms in the Baltic Sea: a multi-sensor approach. Vol. 2, pp. 1211–1213 vol.2.
- Rud, O. and Gade, M., 2000. Using multi-sensor data for algae bloom monitoring. Vol. 4, pp. 1714–1716 vol.4.
- Sun, Y., 1996. Automatic Ice Motion Retrieval from ERS-1 SAR Images Using The Optical Flow Method. *International Journal of Remote Sensing* 17(11), pp. 2059–2087.